

A study of the local entropy generation rate in a porous media burner

I. MOHAMMADI¹⁾, J. A. ESFAHANI^{1,2,3)}, K. C. KIM³⁾

¹⁾*Mechanical Engineering Department, Ferdowsi University of Mashhad, Mashhad, Iran*

²⁾*Center of Excellence on Modelling and Control Systems, (CEMCS), Ferdowsi University of Mashhad, Iran, e-mail: abolfazl@um.ac.ir*

³⁾*School of Mechanical Engineering, Pusan National University, Busan 46241, Republic of Korea*

IN THIS PAPER, THE WORK AND PERFORMANCE of the premixed methane-air porous axisymmetrical burner have firstly been simulated numerically using the CFD tools. For this purpose the set of governing equations has been enriched by an additional energy equation in porous solid, and the chemical species transport has been extended onto the multi-step mechanism (GRI-2-11). This numerical model has been verified on the base of available benchmark experiments. Next, we have studied the local entropy generation problem taking into account not only classical contributions like viscous and turbulent dissipation but also, the porous combustion of gases. The results showed that the greatest portion of entropy generation in the porous medium burner is related to chemical reactions, followed by heat transfer, mass diffusion (mixing) and friction (viscous dissipation), respectively. According to the results, as the excess air ratio increases, the local entropy generation rate due to heat transfer and friction increases and the local entropy generation rate due to chemical reactions is decreased. Also, by increasing the volumetric heat transfer coefficient, the local entropy generation rate due to heat transfer decreases and the local entropy generation rate due to friction and chemical reactions increases. Also, the local entropy generation rate due to mixing does not show a significant change with the changing excess air ratio and volumetric heat transfer coefficient.

Key words: porous media burner, chemical kinetic, volumetric heat transfer, axisymmetric combustion, local entropy generation, excess air ratio.

Copyright © 2020 by IPPT PAN, Warszawa

Notation

A area [m^2],

a emissivity,

C_p fluid heat capacity for constant pressure [$\frac{\text{J}}{\text{kg}\cdot\text{K}}$],

C_B Stefan–Boltzmann constant ($5.67 \cdot 10^{-8}$ [$\frac{\text{W}}{\text{m}^2\cdot\text{K}^4}$]),

D_i mass diffusion coefficient of the i th species,

d_m characteristic diameter [m],

H	volumetric heat transfer coefficient $[\frac{W}{m^3 \cdot K}]$,
h_k	enthalpy of the kth species [J/kg],
K_1	permeability tensor for laminar flow [m ²],
K_2	permeability tensor for turbulent flow [m],
\dot{m}	mass flow rate [kg/s],
N_R	number of reaction [-],
N_S	number of species [-],
PPC	number of pores per cm of the porous medium length,
Q_R	the radiation heat transfer between the solid phase and the environment [W/m ³],
T	temperature [°K],
u	axial velocity [m/s],
v	radial velocity [m/s],
V	velocity vector [m/s],
V_s	superficial velocity [m/s],
W	molecular weight of species [kg/mole],
Y	mass fraction of the species.

Greek letters

ρ	density [kg/m ³],
μ	viscosity [kg/m · s],
ε	porosity [-],
λ_f	fluid conductive heat transfer coefficient [W/m·K],
$\dot{\omega}$	molar rate of reaction of species [mole/m ³ · s],
$\mu_{M,k}$	molar chemical potential [Joule/mole],
v'_k	stoichiometric coefficient of reactant species [-],
v''_k	stoichiometric coefficient of product species [-],
ψ	extinction coefficient [1/m].

Subscript

eff	effective,
f	fluid,
i	transport direction,
in	inlet,
k	species,
s	solid,

1. Introduction

INVESTIGATION OF THE LOCAL ENTROPY GENERATION in transition processes and chemical reactions is important to improve the performance of energy conversion systems. In 1994, DUNBAR *et al.* [1] investigated the sources of combustion irreversibility. They showed that in a combustion process the factors that produce entropy include, the diffusion process where the fuel and air molecules become intrinsically mixed, the chemical reactions (fuel oxidation), internal thermal energy exchange where the product molecules give their kinetic energy to neighboring molecules, and the macromixing process where the system com-

ponents are evenly mixed. In 2002, NISHIDA *et al.* [2] studied entropy generation and exergy loss in the combustion process. They investigated the effects of various fuels, equivalence ratio, and inlet fluid temperature on entropy generation and exergy loss. The results showed that in premixed flames, chemical reactions had the greatest effect on entropy generation and exergy loss, while in diffusion flames, thermal conductivity had the most effect on entropy generation.

In 2005, YAPICI *et al.* [3] computed numerically the local entropy generation due to the high velocity and temperature gradients inside the combustion chamber in methane-air burners. They used the rotational airflow to burn methane fuel with greater efficiency and also examined the effects of the equivalence ratio and swirl number on combustion and entropy generation. In 2005, YAPICI *et al.* [4] performed a numerical study on local entropy generation in a compressible flow through a tube with a sudden expansion. They also studied the effects of mass flux, ambient heat transfer coefficient, and inlet temperature on the entropy generation rate. The results showed that decreasing the radius of the throat significantly increased the maximum amount of volumetric entropy generation rate. In 2006, ABOLFAZLI and JAVADI [5] analyzed the entropy generation of the combustion phenomenon in methane-air furnaces. They found that entropy generation due to friction and diffusion of species was negligible with respect to the contribution of heat transfer and rate of the chemical reaction. Also, the rate of chemical reaction has the highest contribution to the entropy generation in a turbulent flow. In 2007, HOOMAN *et al.* [6] optimized entropy generation and heat transfer in forced convection into the porous saturated duct with a rectangular cross-section. In this study, three different types of boundary conditions were considered and the results were reported for the Nusselt number, the Bejan number, and the dimensionless entropy generation rate based on terms of system parameters. These results make it possible to compare and evaluate the design parameters of rectangular ducts based on terms of heat transfer, pressure drop and entropy generation.

In 2008, BRIONES *et al.* [7] performed entropy generation analysis on the hydrogen-enriched methane-air propagating triple flames. The results showed that as hydrogen is added to methane fuel, entropy generation increases due to increasing thermal conductivity and chemical reactions, and the second law efficiency of the system remains almost constant with the addition of hydrogen. In 2010, RAJIV *et al.* [8] analyzed a laminar, viscous, and incompressible flow through a porous channel. The results indicated that the viscous diffusion had no effect on the entropy generation rate in the centerline of the channel filled with a porous material. In 2011, WAQAR [9] investigated the non-Newtonian fluids in a porous medium. He studied the dilatants and quasi-plastics, and showed the effects of power index, temperature variations, displacement parameter, ax-

ial distance and viscous friction parameter on temperature and velocity profiles, dimensionless entropy generation rate, the ratio of irreversibility and the Bejan number. In 2012, HEIDARY *et al.* [10] investigated the control of free convection and entropy generation in inclined porous media as well as the effects of appendage on the bottom wall. The results showed that this appendage can be used as a control parameter for heat transfer, fluid flow, and entropy generation.

In 2014, ZHOU *et al.* [11] studied optimization of plate-fin heat exchangers by minimizing specific entropy generation rates and found that by increasing the total heat transfer area, reducing the heat transfer rate and increasing the mass flow ratio, the entropy generation rate decreases. In 2014, FEIZ and ESFAHANI [12] investigated the exergy performance of a methane-air cylindrical microcombustor with different inlet conditions (equivalence ratio and inlet velocity). The results showed that entropy generation due to heat transfer had the highest contribution to exergy destruction. Then chemical reactions and mixing have the second highest contribution, respectively. Besides, the results showed that the microcombustor had the lowest irreversibility under stoichiometric conditions.

In 2015, AMANI *et al.* [13] numerically investigated the entropy generation and thermodynamic optimization of the combustion chamber. They examined the effects of various parameters such as the swirl number, the distance between the air nozzle and fuel, the equivalence ratio, the inlet fuel flow rate and the inlet air velocity. The results showed that chemical reactions and heat transfer had the highest contribution to entropy generation and consequently irreversibility.

In 2016, STANCIU *et al.* [14] numerically investigated the entropy generation in micro channels with thermal wells with cross-sections of various shapes. They found that total entropy generation decreased with increasing Reynolds number and also that the channels with square thermal wells had the lowest entropy generation rates compared to circular and hexagonal cross-sections. In the same year, TORABI *et al.* [15] reviewed the entropy generation in thermal systems with solid structures. They studied the recent advances in the second law analyses of these systems with an emphasis on the theoretical and modeling aspects, they also studied the effects of including solid components on the entropy generation within different thermal systems and finally investigated the mathematical methods used in this branch of thermodynamic. In other work in 2017, they presented the challenges and progress on the modeling of entropy generation in porous media. They investigated the recent developments of the second law investigations in porous media and the effects of various parameters on the entropy generation in porous systems. They also focused on the local equilibrium and non-equilibrium upon the second law performance and mathematical methods that have been used for second law simulations [16].

In 2019, RAHBAR *et al.* [17] investigated an analytical study of entropy generation in rectangular natural convective porous fins. The results of solving these equations showed that the entropy generation number is a function of S_H , temperature ratio and non-dimensional local temperature of the porous fin. The results also indicated that, for both long and insulated porous fins, at given values of S_H and the temperature ratio, the maximum entropy production occurs at the base of the fins with the maximum values of temperature difference.

According to the aforementioned literature survey, only few theoretical and practical studies have been done on the local entropy generation rate in the porous medium burner. In this work, such a combustion system is examined using the same configuration of the burner as in a recent paper [18] where, essentially, changing continuous porosity has been used for a constant value of excess air ratio and volumetric heat transfer coefficient, and the effects of these two very important parameters on the entropy generation rate have not been investigated. Therefore, the present work is meant to complement and extend that recent study.

2. Mathematical model

2.1. Burner geometry

In this study, the numerical solution of the local entropy generation in incompressible flow through a porous media burner is analyzed. The two-dimensional axisymmetric model of the considered burner is shown in Fig. 1. It is assumed that the wall of the preheating zone is adiabatic and the wall of the combustion zone is under the constant temperature conditions (at 1410 K). The lengths of the preheating zone and the combustion zone are 20 mm and 110 mm, respectively and the divergence length that is a part of the combustion zone, is 10 mm. the radiuses of the burner at inlet and outlet are constant and equal to 13 mm and 15 mm, respectively.

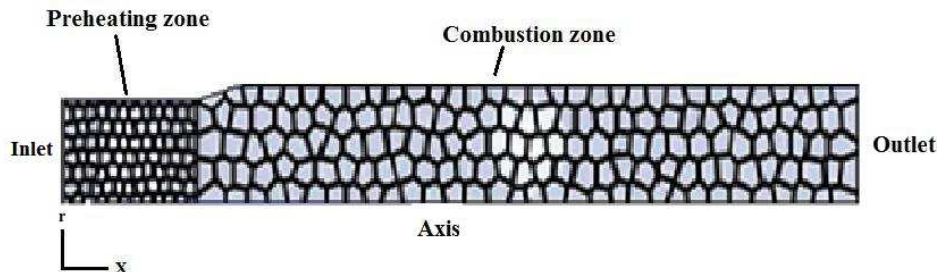


FIG. 1. The schematic of the burner geometry.

Table 1 shows the values of the thermal conductivity coefficient, the convective heat transfer coefficient, and the diameter of the pore used in the preheating and combustion zones.

Table 1. Thermophysical and thermo chemical properties of porous material used in this work [19, 20].

Properties	Preheating zone	Combustion zone
Conductive coefficient [W/mK]	0.1	0.5
Convective coefficient [W/m ³ K]	1×10^7	1×10^8
Pore diameter [mm]	0.55	0.6
Porosity [-]	0.7	0.85

The assumptions made are as follows:

1. Steady-state condition, laminar and Newtonian fluid are assumed.
2. The effects of body forces, the catalytic effect of porous material at high temperatures and the effects of Soret and Dufour are negligible.
3. The radiative heat transfer of the gas phase against the solid matrix is ignored.

The governing conservation equations [19, 21–24].

Continuity equation

$$(2.1) \quad \text{div}(\rho \vec{V}_s) = 0.$$

Axial momentum equation

$$(2.2) \quad \text{div}(\rho u \vec{V}_s) = \text{div}(\mu \nabla u) - \frac{\partial p}{\partial x} - \left(\frac{\Delta P}{\Delta L} \right)_x.$$

Radial momentum equation

$$(2.3) \quad \text{div}(\rho v \vec{V}_s) = \text{div}(\mu \nabla v) - \frac{\partial p}{\partial r} - \left(\frac{\Delta P}{\Delta L} \right)_r.$$

In the momentum equations, an additional pressure drop has to be considered, which depends on the properties of the porous medium. Second-order polynomials are used to describe this pressure drop. According to the Forchheimer equation for the *i*th direction, we have [19, 21, 22, 25, 26].

The pressure drop equation

$$(2.4) \quad \left(\frac{\Delta P}{\Delta L} \right)_i = \frac{\mu}{K_1} (V_s)_i + \frac{\mu}{K_2} (V_s)_i |(\vec{V}_s)|.$$

Superficial velocity

$$(\vec{V}_s) = \varepsilon(\vec{V}).$$

Permeability for Darcy flow

$$K_1 = \frac{(d_m)^2 \varepsilon^3}{180\mu(1 - \varepsilon)^2}.$$

Permeability for Forchheimer flow

$$K_2 = \frac{(d_m)\varepsilon^3}{1.8\rho_f(1 - \varepsilon)}.$$

Gas-phase energy

$$(2.5) \quad \text{div}(\rho\vec{V}_s C_p T_f) = \text{div}(\varepsilon\lambda_f \text{grad}(T_f)) + H(T_s - T_f) - \varepsilon \sum_{K=1}^{N_s} \dot{\omega}_k h_k.$$

Solid phase energy

$$(2.6) \quad \text{div}((1 - \varepsilon)\lambda_{\text{eff}_i} \text{grad}(T_s)) + H(T_f - T_s) - Q_R \delta = 0.$$

Effective thermal conductivity [20, 23, 27–29]

$$\lambda_{\text{eff}_i} = \lambda_{\text{eff}}^{\circ} + \frac{\dot{m} C_p d}{K_i}.$$

Radiation heat transfer between the solid phase and environment [23]

$$Q_R = (1 - \varepsilon) \frac{a C_B (T_s^4 - T_0^4)}{\Delta l} e^{-\psi x}.$$

Extinction coefficient for the porous matrix

$$\psi = -\frac{1}{\Delta l} \ln \varepsilon.$$

Temperature of the environment was taken to be $T_0 = 288^\circ\text{K}$.

The volumetric heat transfer coefficient [30–33]

$$H = a_v h,$$

a_v is the cross-sectional area per unit volume of porous material that this coefficient can be experimentally determined [34]

$$a_v = 169.4PPC \quad (\text{Pore Per Centimeter}),$$

and δ parameter in Eq. (2.6) is defined as follow:

$$\delta = \begin{cases} 1 & \text{elsewhere,} \\ 0 & \text{inlet \& outlet.} \end{cases}$$

Species conservation equations

$$(2.7) \quad \text{div}(\rho \vec{V}_s Y_k) = \text{div}(\rho \varepsilon D_{km} \text{grad}(Y_k)) + \varepsilon \dot{\omega}_k, \quad k \in [1, N_s].$$

The terms of the production and conversion of species k due to the chemical reactions appear as source/sink terms in the gas phase energy and the chemical species transfer equations.

$$\dot{\omega}_k = M_k \sum_{l=1}^{N_R} (\nu''_{kl} - \nu'_{kl}) K_1 \cdot \left(\prod_{\text{reactants}} C^{\nu'_{kl}} - \frac{1}{K_c} \prod_{\text{products}} C^{\nu''_{kl}} \right)$$

where ν'_{kl} and ν''_{kl} are the stoichiometric coefficients and must be satisfied with the following equation

$$\sum_{k=1}^{N_s} \nu'_{kl} A_k \leftrightarrow \sum_{k=1}^{N_s} \nu''_{kl} A_k,$$

and K_1 is the reaction rate coefficient and is defined by the Arrhenius expression [35]

$$K_1 = K_1^0 T^{\beta_1} \exp\left(-\frac{E_1}{RT}\right)$$

where all of the parameters are defined in the notation.

Gas-phase thermochemical and transport properties are calculated by subroutine TRANFIT [36] and thermodynamic database of the CHEMKIN library. All simulations are conducted for premixed methane/air mixture and multi-step chemical kinetics GRI 2.11 that includes 49 species and 279 chemical reactions.

The inlet, outlet, and the boundary conditions are given by:

Inlet:

$$u = u_{\text{in}}, \quad v = 0, \quad T_f = T_{f,\text{in}}, \quad Y_i = Y_{i,\text{in}}, \\ (1 - \varepsilon) \lambda_s \frac{\partial T_s}{\partial x} = -\varepsilon_r \sigma (T_s^4 - T_o^4).$$

Outlet:

$$\frac{\partial u}{\partial x} = \frac{\partial v}{\partial x} = \frac{\partial T_f}{\partial x} = \frac{\partial Y_i}{\partial x} = 0, \\ (1 - \varepsilon) \lambda_s \frac{\partial T_s}{\partial x} = -\varepsilon_r \sigma (T_s^4 - T_o^4).$$

On the axis:

$$\frac{\partial u}{\partial r} = \frac{\partial T_f}{\partial r} = \frac{\partial T_s}{\partial r} = \frac{\partial Y_i}{\partial r} = 0, \quad v = 0.$$

At the wall of the burner the no-slip condition is applied.

2.2. The rate of entropy production

Local entropy generation due to heat transfer [13, 37–39]

$$(2.8) \quad (S'''_{\text{gen}})_{\text{heat}} = \frac{\varepsilon \lambda_f}{T_f^2} \cdot \left[\left(\frac{\partial T_f}{\partial x} \right)^2 + \left(\frac{\partial T_f}{\partial r} \right)^2 \right] \\ + \frac{(1 - \varepsilon) \lambda_{\text{eff}x}}{T_s^2} \cdot \left(\frac{\partial T_s}{\partial x} \right)^2 + \frac{(1 - \varepsilon) \lambda_{\text{eff}r}}{T_s^2} \cdot \left(\frac{\partial T_s}{\partial r} \right)^2.$$

Local entropy generation due to friction [13, 37–39]

$$(2.9) \quad (S''_{\text{gen}})_{\text{fric}} = \frac{\mu}{T} \cdot \emptyset.$$

Viscous dissipation

$$\emptyset = 2 \cdot \left[\left(\frac{\partial u_x}{\partial x} \right)^2 + \left(\frac{\partial u_r}{\partial r} \right)^2 + \left(\frac{u_r}{r} \right)^2 \right] + \left(\frac{\partial u_x}{\partial r} + \frac{\partial u_r}{\partial x} \right)^2.$$

Local entropy generation due to mixing [40]

$$(2.10) \quad (S'''_{\text{gen}})_{\text{mixing}} = \sum_{i=1}^N \rho D_{\text{im}} \left[\frac{R_i}{p} \frac{\partial Y_i}{\partial x_a} \frac{\partial P}{\partial x_a} + \frac{R_i}{Y_i} \frac{\partial Y_i}{\partial x_a} \frac{\partial Y_i}{\partial x_a} \right] > 0.$$

Local entropy generation due to chemical reactions [41]

$$(2.11) \quad (S'''_{\text{gen}})_{\text{reaction}} = \frac{A\omega}{T} = \frac{\omega}{T} \sum_{i=1}^N (v'_i - v''_i) \mu_{M,i} > 0.$$

The total entropy generation rate

$$(2.12) \quad \dot{S}_{\text{gen}} = \oint S'''_{\text{gen}} r \partial \theta \cdot \partial r \cdot \partial x.$$

3. Validation of results

As shown in Table 2, the validity of the numerical model is examined by comparing the adiabatic temperatures predicted by our numerical simulation in a porous medium burner at an input velocity of 50 cm/s for different values of

Table 2. Comparison of adiabatic flame temperature between the present work and [42].

Equivalence ratio with input velocity $50 \frac{\text{cm}}{\text{s}}$	1	1.1	1.2
Experimental adiabatic flame temperature [K] ([42])	2230	2200	2140
Calculated adiabatic flame temperature [K]	2311	2298	2301
Errors %	3.51	4.26	6.99

the equivalence ratio with the adiabatic flame temperature for CH_4 -air mixtures which is reported in TURNS [42]. As can be seen, by decreasing the equivalence ratio, the difference between numerical and experimental results are reduced, which can be discounted in engineering works.

In Fig. 2, the mass fraction of NO species for the results of numerical and experimental simulations in a 5 kW burner and at the output of the burner as a function of the excess air ratio is shown. GRI-2.11 kinetics is used for a numerical simulation. The greatest difference between the experimental and the numerical simulation results is about 7%. It is necessary to use a detailed chemical mechanism and temperature field in order to obtain a better prediction of NO emission. According to Fig. 2, there is little difference between the results of numerical simulations and experimental results that can be ignored.

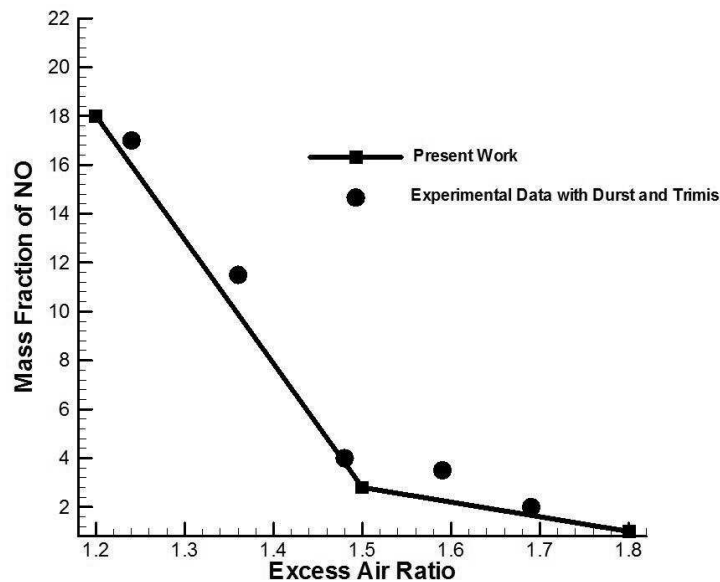


FIG. 2. Comparison of NO species with experimental results in a porous media burner and GRI-2.11 chemical kinetics for different amounts of the excess air ratio [43].

Grid independence test

To check mesh independence, a different grid size was investigated. The results showed that the variations of the variables with the grid smaller than 260×26 are about 3% which can often be neglected in engineering work, so all results are reported based on the mesh mentioned.

4. Results and discussion

In the present work, a two-dimensional axisymmetric numerical model for premixed methane-air combustion in porous media has been developed. For this purpose, multi-step mechanism GRI.2.11 which includes 49 species and 279 chemical reactions and constant porosity have been used and the effects of them on the temperature profile and local entropy generation rate have been investigated. This model solves the continuity equation, Navier Stokes equations, the solid and gas energy equations, and the chemical species transport equations by using the finite volume method, and the pressure and velocity have been coupled with the SIMPLE algorithm. After convergence, local entropy generation rate equations, are solved by considering the values of temperature and velocity and concentration of chemical species. In this paper, the effects of volumetric heat transfer coefficient and excess air ratio on the local entropy generation rate have been shown.

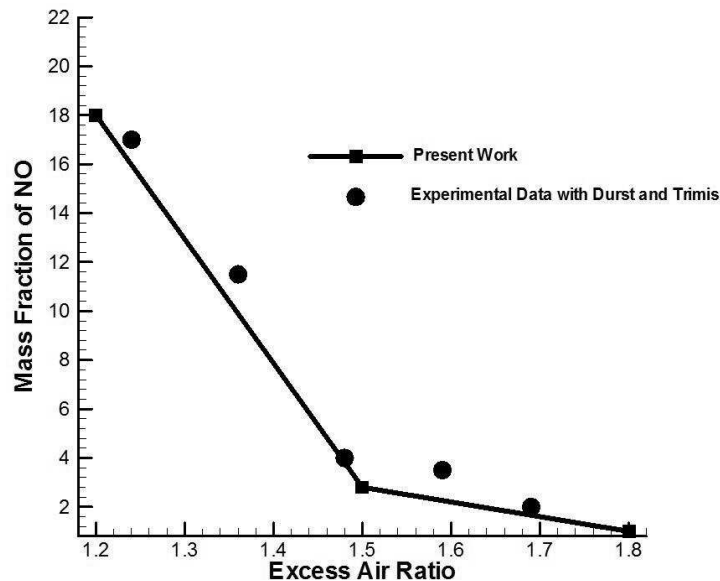


FIG. 3. Gas temperature profile on the centerline of the burner for different values of excess air ratio.

Figure 3 shows the gas temperature profile for different values of the excess air ratio. As can be seen by increasing the excess air ratio, the flow rate increases, which results in better cooling of the porous material in the upstream region, causing the flame front to move downstream and to reduce the maximum temperature value. However, the outlet temperature values for the different values of the excess air ratio are approximately the same.

Figure 4 shows the local entropy generation rate due to heat transfer for different values of the excess air ratio. According to Fig. 4 the least entropy gen-

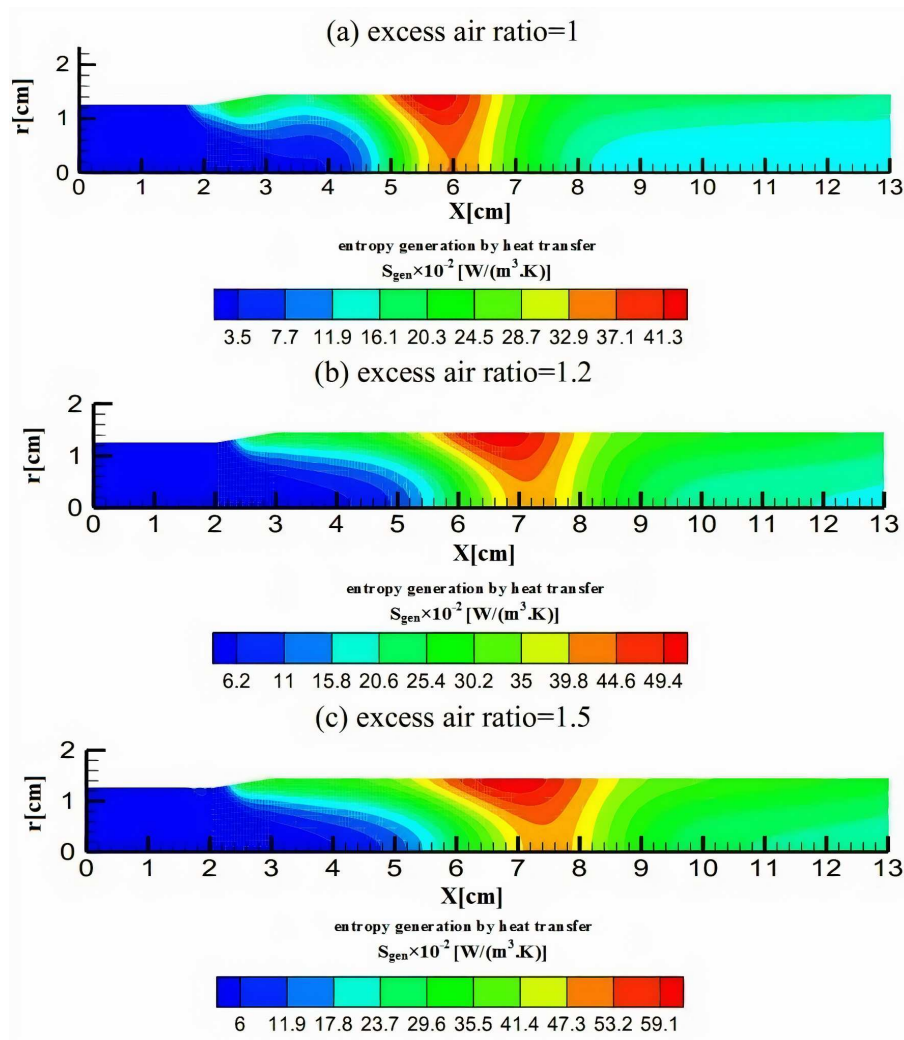


FIG. 4. Local entropy generation rate due to heat transfer for different values of excess air ratio.

eration occurs for the excess air ratio 1, this can be explained by the fact that according to Eq. (2.8), local entropy generation due to heat transfer is inversely proportional to the square of the temperature and, according to Fig. 3, the maximum temperature occurs for the stoichiometric condition (excess air ratio = 1). As can be seen in Fig. 4, the maximum amount of local entropy generation happens near the wall with high-temperature gradients and this maximum value is transferred downstream by increasing the excess air ratio.

Figure 5 shows the local entropy generation rate contour due to friction for different values of excess air ratio. According to Fig. 5 the least entropy

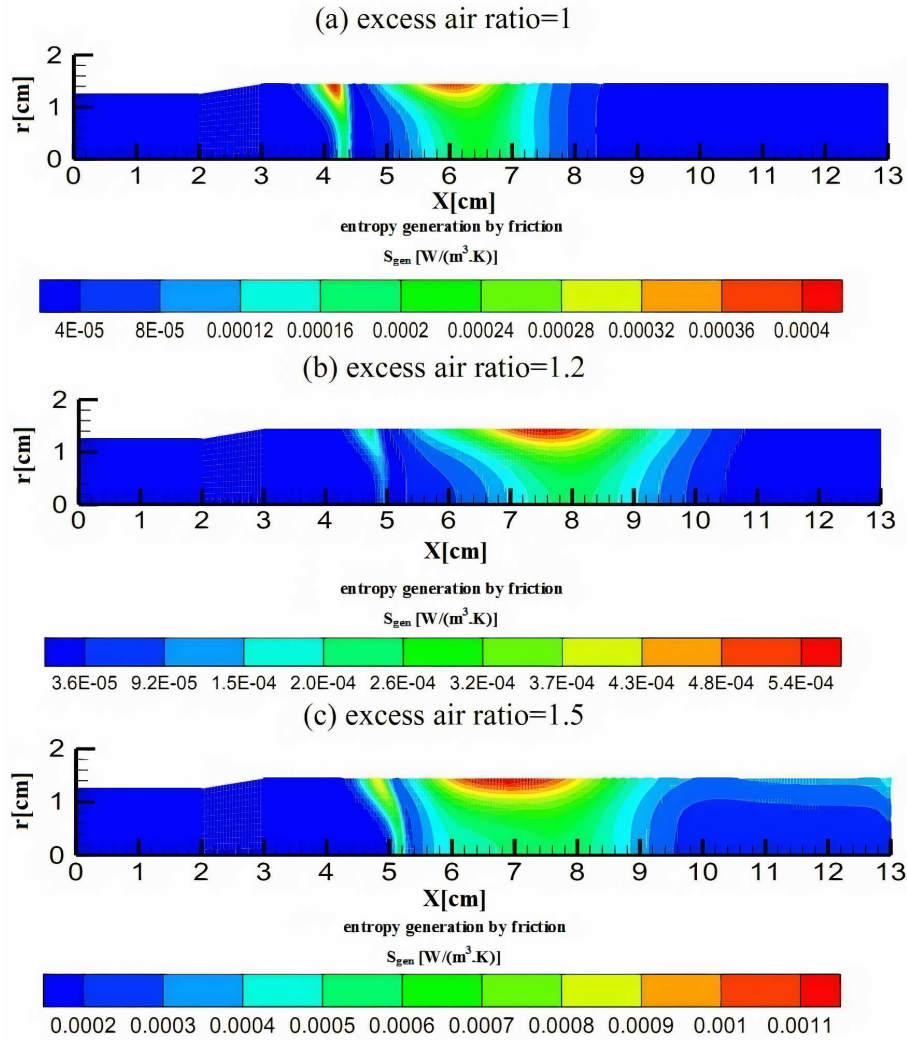


FIG. 5. Local entropy generation rate due to friction for different values of excess air ratio.

generation occurs for the excess air ratio 1, this can be explained by the fact that according to Eq. (2.9), local entropy generation due to friction is inversely proportional to the temperature and by increasing the temperature, the amount of local entropy generation due to friction decreases. It is clear that the local entropy generation rate due to friction is thousands of times lower than other sources of entropy generation and can be neglected.

Figure 6 shows the local entropy generation rate due to chemical reactions for different values of excess air ratio. Compared to the thermal entropy generation rate, the local entropy generation rate due to chemical reactions is higher. The

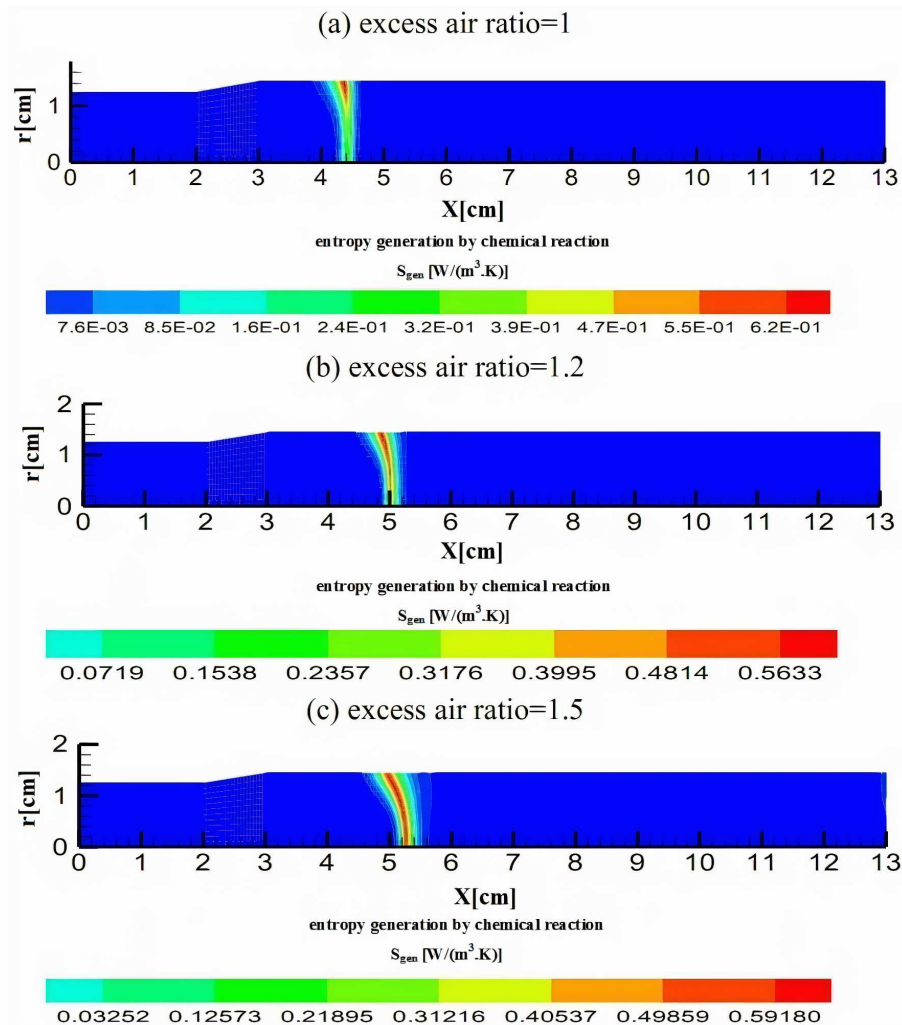


FIG. 6. Local entropy generation rate due to chemical reactions for different values of excess air ratio.

conversion of reactants into products in the combustion zone causes the highest local entropy generation rate due to chemical reactions.

According to the figure, the highest amount of local entropy generation due to chemical reactions occurs for the excess air ratio 1. It can be added that according to Eq. (2.11), the local entropy generation rate is inversely proportional to temperature, but it is observed that the highest amount of local entropy generation via chemical reactions happens at the excess air ratio 1 that has the highest temperature. The cause can be related to other parameters such as chemical potential and the rate of production or consumption of species.

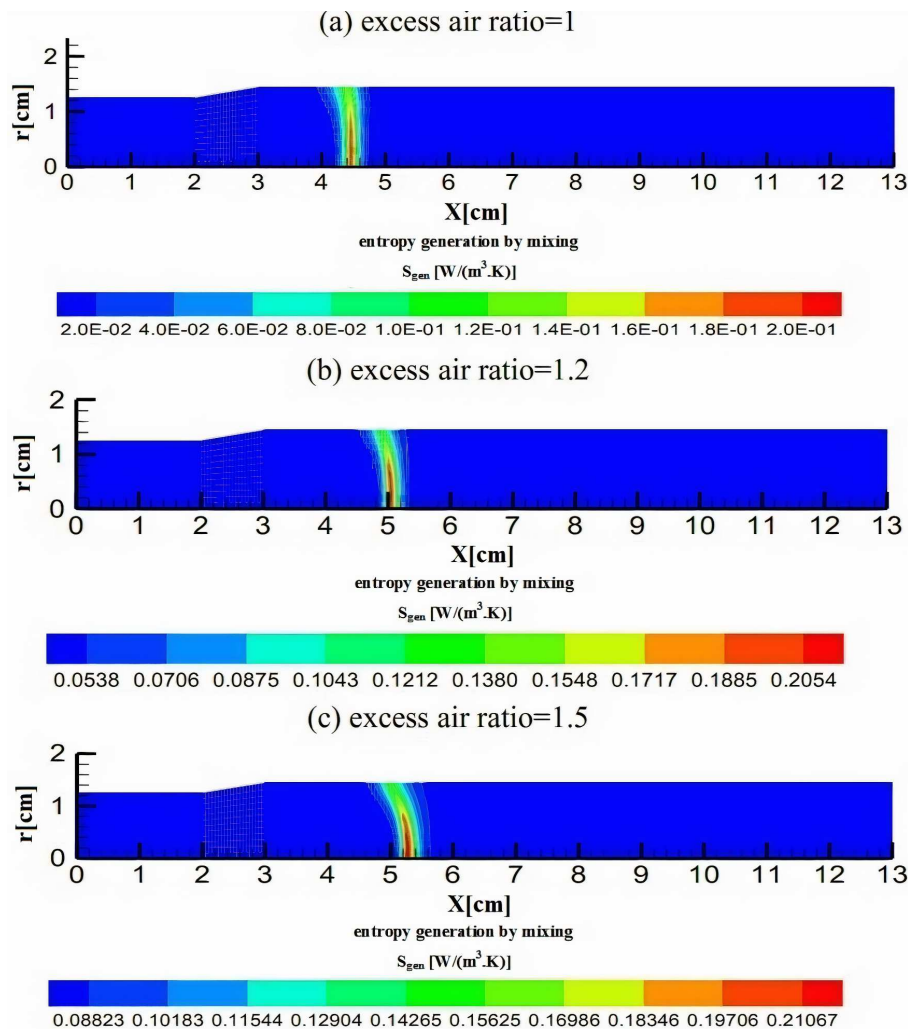


FIG. 7. Local entropy generation rate due to mixing for different values of excess air ratio.

According to the figure, as the excess air ratio increases, the location of maximum local entropy generation is transferred downstream.

Figure 7 shows the local entropy generation rate due to mixing for different values of excess air ratio. Considering the figure, as the excess air ratio increases, there is no significant change in the local entropy generation rate.

Figure 8 shows the gas temperature profiles for different values of the volumetric heat transfer coefficient. According to the figure, with increasing the volumetric heat transfer coefficient the gas temperature increases. As the volumetric heat transfer coefficient increases, the flame front moves upstream.

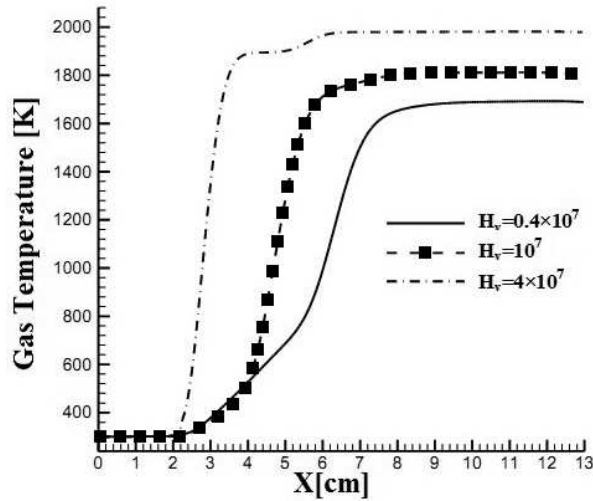


FIG. 8. Gas temperature profile on the centerline of the burner for different values of volumetric heat transfer H_v .

Figure 9 shows the contour of the local entropy generation rate due to heat transfer for different values of the volumetric heat transfer coefficient. As the volumetric heat transfer coefficient increases, the gas temperature increases and consequently the amount of local entropy generation decreases.

Figure 10 shows the contour of the local entropy generation rate due to friction for different values of the volumetric heat transfer coefficient. By increasing the volume heat transfer coefficient the local entropy generation rate due to friction increases quantitatively.

Figure 11 shows the local entropy generation rate via mixing for different values of the volumetric heat transfer coefficient. As the volumetric heat transfer coefficient decreases, the reaction rate increases and the flame thickness decreases, which results in very high concentration gradients in the combustion

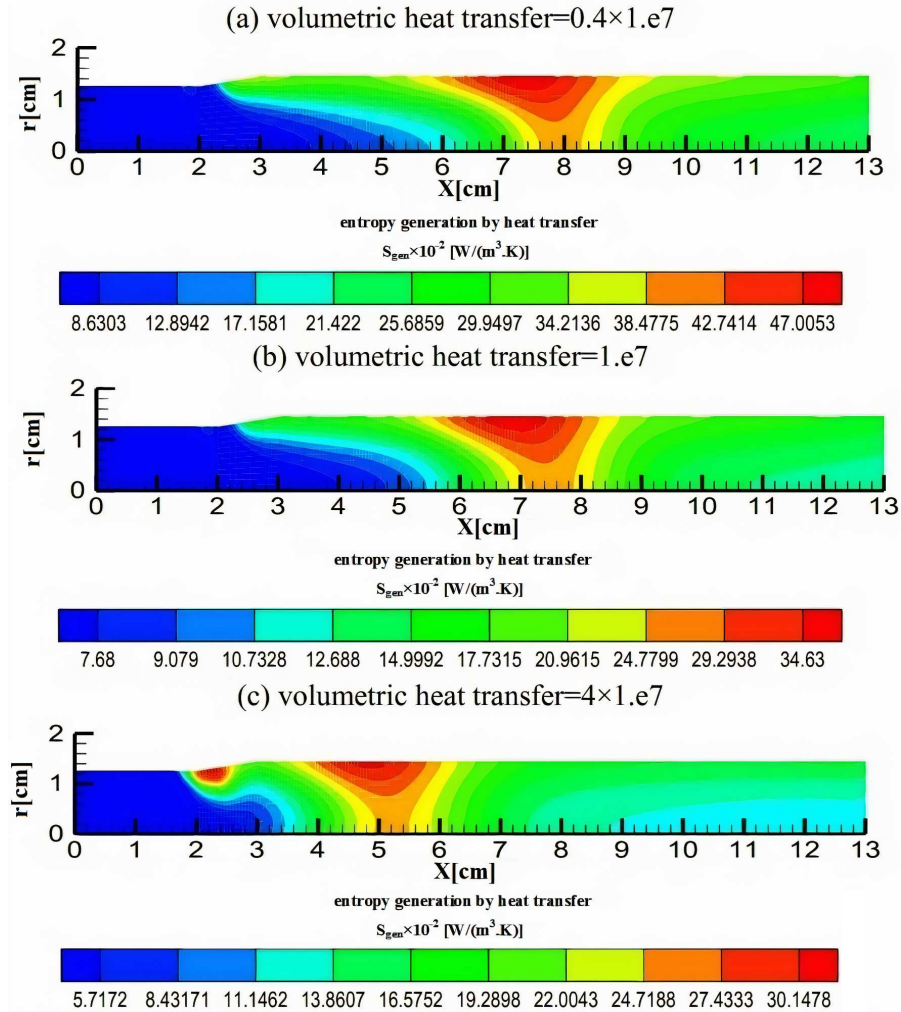


FIG. 9. Local entropy generation rate due to heat transfer for different values of volumetric heat transfer.

zone. On the other hand, as the reaction rate increases, the concentration of each species increases. This phenomenon in the local entropy generation due to mixing according to Eq. (2.10) acts as the opposite and causes the value of this parameter to remain unchanged.

Figure 12 shows the local entropy generation rate due to chemical reactions for different values of the volumetric heat transfer coefficient. According to the figure, with increasing volumetric heat transfer coefficient, the local entropy generation rate increases rapidly.

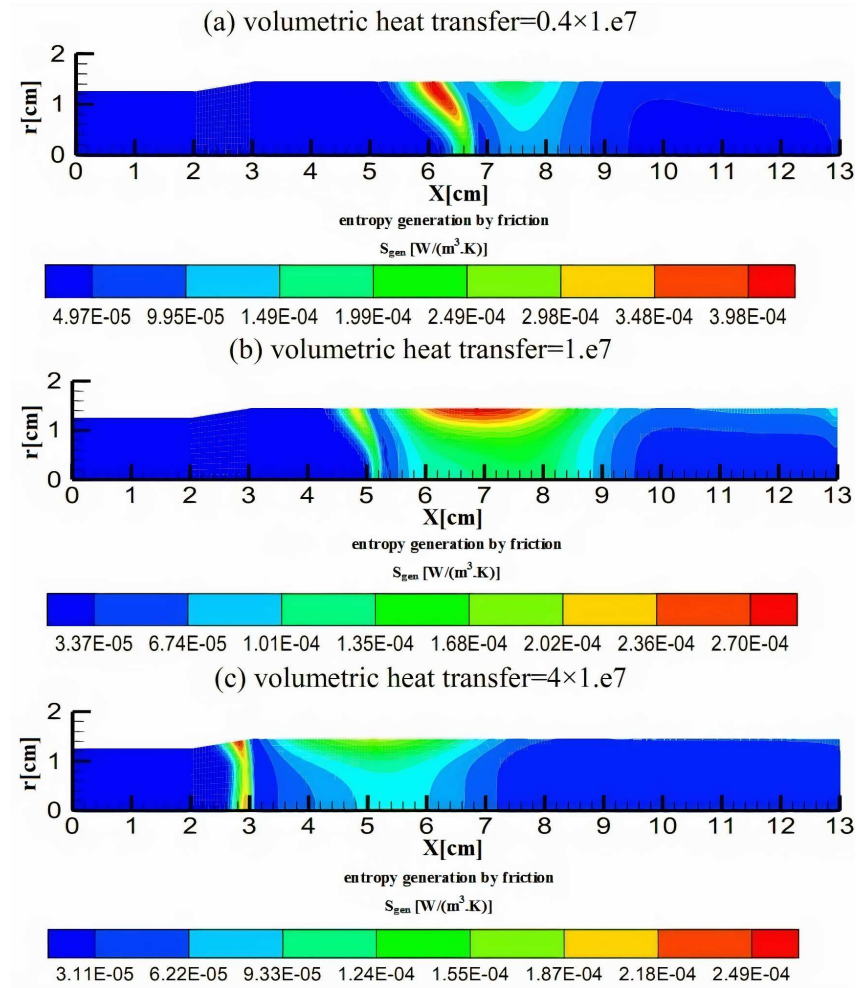


FIG. 10. Local entropy generation rate due to friction for different values of volumetric heat transfer.

5. Conclusions

1. In premixed flames, the local entropy generation rate due to chemical reactions and heat transfer plays a major role and the rate of local entropy generation due to friction can be neglected. Therefore, to reduce the total entropy generation, the contribution due to heat transfer and chemical reactions should be reduced as far as possible.
2. By taking into account chemical kinetics, most of the entropy generation factors in the porous media burner are chemical reactions, followed by heat transfer, mixing and friction, respectively.

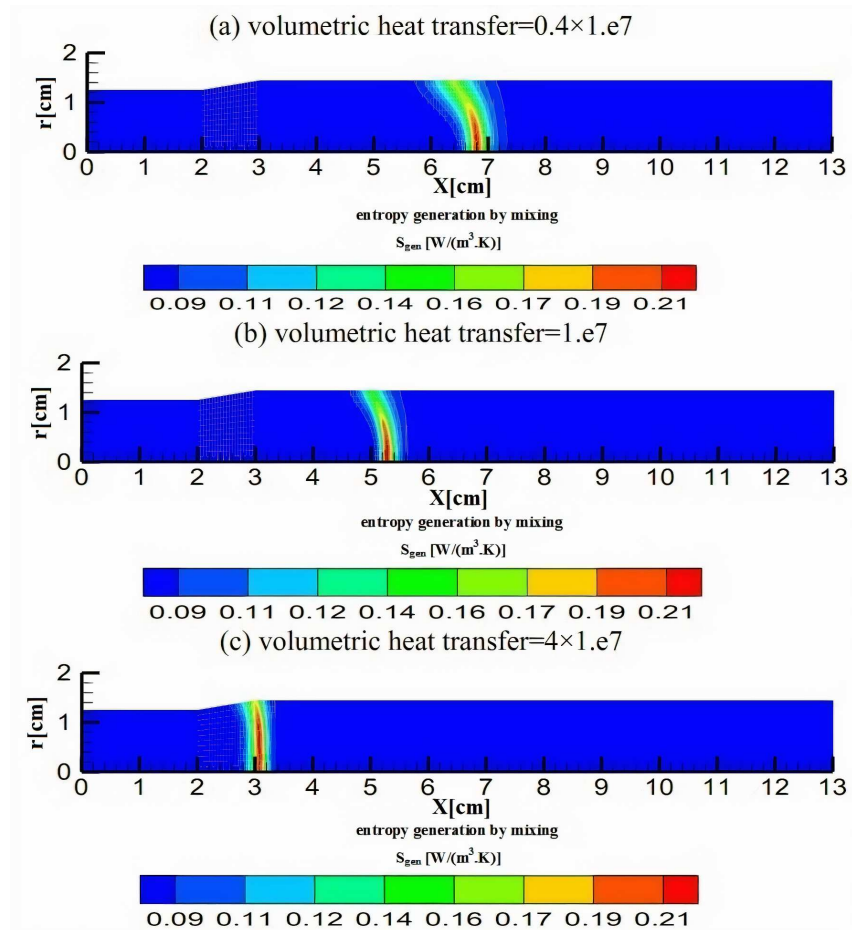


FIG. 11. Local entropy generation rate due to mixing for different values of volumetric heat transfer.

3. By increasing the excess air ratio, the local entropy generation rate due to heat transfer and friction is increased and the local entropy generation rate due to chemical reactions is decreased.
4. By increasing the volumetric heat transfer coefficient, the local entropy generation rate due to heat transfer decreases and the local entropy generation rate due to friction and chemical reactions increases.
5. The local entropy generation rate due to mixing operates independently of the excess air ratio and the volumetric heat transfer coefficient and does not change with the change of them.

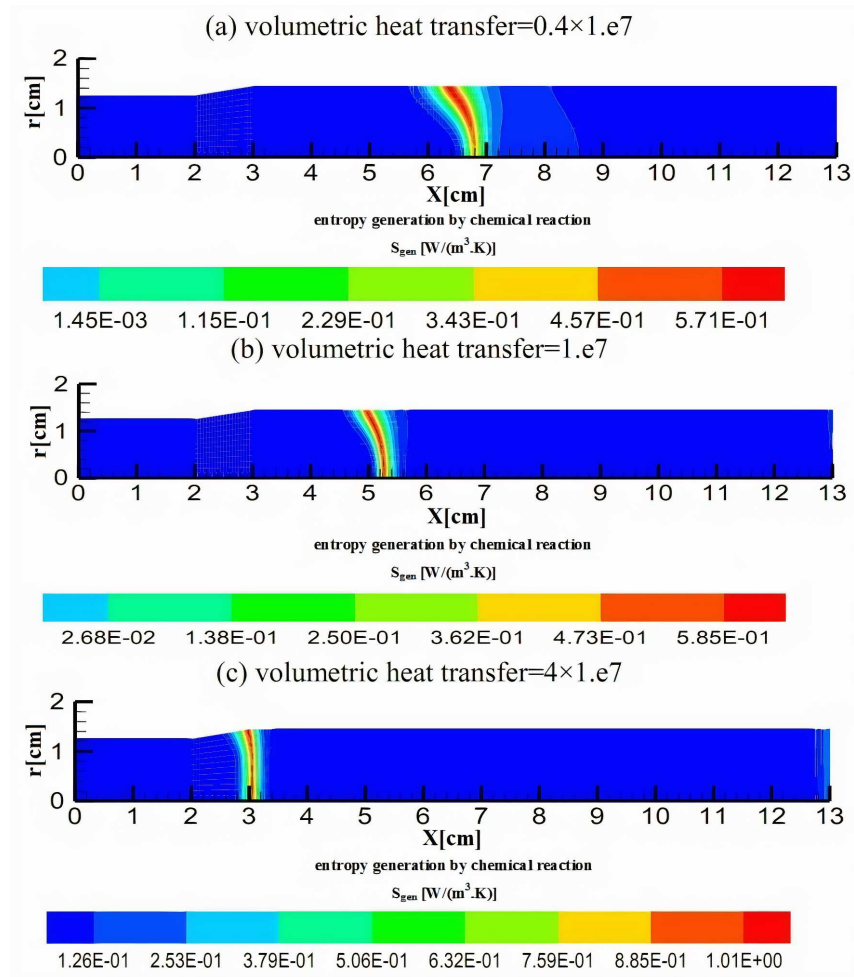


FIG. 12. Local entropy generation rate due to chemical reactions for different values of volumetric heat transfer.

Due to the importance of coefficients of excess air ratio and volume heat transfer, it is observed that entropy generation due to heat transfer decreases by decreasing excess air ratio and increasing volumetric heat transfer coefficient, while entropy generation due to chemical reactions decreases by increasing excess air ratio and decreasing volumetric heat transfer coefficient, and because they behave in a completely opposite way, in order to determine the best practical coefficients, optimization must be done.

Author contribution statement

All the authors have the same contribution to this article.

Acknowledgments

This work was supported by Brain Pool Program through the National Research Foundation of Korea (NRF) funded by the Ministry of Science and ICT (NRF-2019H1D3A2A01102198).

References

1. W.R. DUNBAR, N. LIOR, *Sources of combustion irreversibility*, Combustion Science and Technology, **103**, 41–61, 1994.
2. N. KOUSUKE, T. TOSHIMI, K. SHINICHI, *Analysis of entropy generation and exergy loss during combustion*, Proceedings of the Combustion Institute, **29**, 869–874, 2002.
3. H. YAPICI, N. KAYATAŞ, B. ALBAYRAK, G. BAŞTÜRK, *Numerical calculation of local entropy generation in a methane-air burner*, Energy Conversion and Management, **46**, 1885–1919, 2005.
4. H. YAPICI, N. KAYATAŞ, N. KAHRAMAN, G. BAŞTÜRK, *Numerical study on local entropy generation in compressible flow through A suddenly expanding pipe*, Entropy, **7**, 38–67, 2005.
5. J.A. ESFAHANI, M. JAVADI, *The analysis of the entropy generation of the combustion phenomenon in methane-air burner*, Second Iranian Combustion Conference, 1386.
6. K. HOOMAN, H. GURGENCI, A.A. MERRIKH, *Heat transfer and entropy generation optimization of forced convection in a porous-saturated duct of rectangular cross-section*, International Journal of Heat and Mass Transfer, **50**, 2051–2059, 2007.
7. A. M. BRIONES, A. MUKHOPADHYAY, S.K. AGGARWAL, *Analyses of entropy generation in hydrogen-enriched methane-air propagating triple flames*, International Journal of Hydrogen Energy, **34**, 1074–1083, 2009.
8. D. RAJIV, S.P. SINGH, B.B. SINGH, *Analysis of incompressible viscous laminar flow through a channel filled with porous media*, International Journal of Stability and Fluid Mechanics, **1**, 127–134, 2010.
9. A.K. WAQAR, *Entropy generation in non-newtonian fluids along a horizontal plate in porous media*, Journal of Thermophysics and Heat Transfer, **25**, 298–303, 2011.
10. H. HEIDARY, M. PIRMOHAMMADI, M. DAVOUDI, *Control of free convection and entropy generation in inclined porous media*, Heat Transfer Engineering, **33**, 565–573, 2012.
11. Y. ZHOU, L. ZHU, J. YU, Y. LI, *Optimization of plate-fin heat exchangers by minimizing specific entropy generation rate*, International Journal of Heat and Mass Transfer, **78**, 942–946, 2014.
12. M.E. FEYZ, J.A. ESFAHANI, *Energetic performance of a cylindrical methane-air micro combustor under various inlet conditions*, International Journal of Exergy, **15**, 257–275, 2014.
13. A. AMANI, H.R. ARJMANDI, *A numerical investigation of the entropy generation in and thermodynamic optimization of a combustion chamber*, Energy, **81**, 706–718, 2015.

14. D. STANCIU, A.A. ALFARYJAT, A. DOBROVICESCU *et al.*, *Numerical investigation of entropy generation in micro-channels heat sink with different shapes*, 7th International Conference on Advanced Concepts in Mechanical Engineering, Iasi, Romania, 2016.
15. M. TORABI, K. ZHANG, N. KARIMI, G.P. PETERSON, *Entropy generation in thermal systems with solid structures – A concise review*, International Journal of Heat and Mass Transfer, **97**, 917–931, 2016.
16. M. TORABI, N. KARIMI, G.P. PETERSON, S. YEE, *Challenges and progress on the modelling of entropy generation in porous media: A review*, International Journal of Heat and Mass Transfer, **114**, 31–46, 2017.
17. S.M. KHATAMI, N. RAHBAR, *An analytical study of entropy generation in rectangular natural convective porous fins*, Thermal Science and Engineering Progress, **11**, 142–149, 2019.
18. I. MOHAMMADI, H. AJAM, *A theoretical study of entropy generation of the combustion phenomenon in the porous medium burner*, Energy, **188**, 116016–116004, 2019.
19. S.C. MISHRA, M. STEVEN, S. NEMODA *et al.*, *Heat transfer analysis of a two-dimensional rectangular porous radiant burner*, International Communication in Heat and Mass Transfer, **33**, 467–474, 2006.
20. E.U. SCHLÜNDER, E. TSOTSAS, *Wärmeübertragung in Festbetten, druchmischten Schüttgütern und Wirbelschichten*, Georg Thieme Verlag, Stuttgart-NewYork, 1988.
21. M. FARZANEH, R. EBRAHIMI, M. SHAMS, M. SHAFIEY, *Two-dimensional numerical simulation of combustion and heat transfer in porous burners*, Engineering Letters, **15**, 370–375, 2007.
22. I. MALICO, X.Y. ZHOU, J.C.F. PEREIRA, *Two-dimensional numerical study of combustion and pollutants formation in porous burners*, Combustion Science and Technology, **152**, 57–79, 2000.
23. S. NEMODA, D. TRIMIS, G. ZIVKOVICH, *Numerical simulation of porous burners and hole plate surface burners*, Journal of Thermal Science, **1**, 3–17, 2004.
24. C.J. TSENG, *Effect of hydrogen addition on methane combustion in a porous medium burner*, International Journal of Hydrogen Energy, **27**, 699–707, 2002.
25. S. ERGUN, *Fluid flow through packed columns*, Chemical Engineering Progress, **48**, 89–94, 1952.
26. I.F. MACDONALD, M.S. EI-SAYED, K. MOW, F. A. L. DULLIEN, *Flow through porous media ergun equation revisited*, Industrial & Engineering Chemistry Fundamentals, **18**, 199–208, 1979.
27. M.A. MUJEEBU, M. ABDULLAH, A. MOHAMAD, *Development of energy efficient porous medium burners on surface and submerged combustion modes*, Energy, **36**, 5132–5139, 2011.
28. H.L. PAN, O. PICKENÄCKER, K. PICKENÄCKER, D. TRIMIS, T. WEBER, *Experimental determination of effective heat conductivities of highly porous media*, 5th European Conference on Industrial Furnaces and Boilers, Porto, 11–14, 2000.
29. K. VAFAI, *Handbook of Porous Media*, 2nd ed., Taylor & Francis Group, LLC USA, 2005.

30. X. FU, R. VISKANTA, J.P. GORE, *Measurement and correlation of volumetric heat transfer coefficients of cellular ceramics*, Experimental Thermal and Fluid Science, **17**, 285–293, 1998.
31. M. KAVIANY, *Principles of Heat Transfer in Porous Media*, 2nd ed., Springer-Verlag, New York, 1999.
32. R. VISKANTA, *Interaction of combustion and heat transfer in porous inert media*, Transport Phenomena in Combustion, **1**, 64–87, 1996.
33. L.B. YOUNIS, R. VISKANTA, *Experimental determination of the volumetric heat transfer coefficient between steam of air and ceramic foam*, International Journal of Heat Mass Transfer, **36**, 1425–1434, 1993.
34. L.A. CATALANO, A. DADONE, D. MANODORO, A. SAPONARO, *Efficient design optimization of duct-burners for combined cycle and cogenerative plants*, Engineering Optimization, **38**, 801–820, 2006.
35. R.J. KEE, F.M. RUPLEY, J.A. MILLER, *The Chemkin thermodynamic data base*, Sandia National Laboratories, Report SAND-8215B, 1992.
36. R.J. KEE, G. DIXON-LEWIS, J. WARNATZ, M. E. COLTRIN, J. A. MILLER, *A Fortran computer code package for the evaluation of gas-phase multi-component transport properties*, Sandia National Laboratories Report SAND86-8246, 1986.
37. A. BEJAN, *Second law analysis in heat transfer*, Energy, **5**, 721–732, 1980.
38. A. BEJAN, *Entropy Generation Through Heat and Fluid Flow*, John Wiley & Sons, Canada, 1994.
39. A. BEJAN, *Entropy Generation Minimization*, CRC Press, USA, 71–109, 1996.
40. E. MIRANDA, *Entropy generation in a chemical reaction*, European Journal of Physics, **31**, 267–272, 2012.
41. F.M. WHITE, *Viscous Fluid Flow*, 2nd ed., p. 614, McGraw-Hill Series in Mechanical Engineering, 1991.
42. S.R. TURNS, *An Introduction to Combustion*, McGraw Hill International Editions, Singapore, 2000.
43. F. DURST, D. TRIMIS, *Compact porous medium burner and heat exchanger for household applications*, EC Project Report (contract no. JOE3-CT95-0019), 1996.

Received November 7, 2019; revised version May 23, 2020.

Published online June 30, 2020.
